Nano Energy 38 (2017) 185–192

Contents lists available at ScienceDirect

Nano Energy

journal homepage: www.elsevier.com/locate/nanoen

Full paper

Self-powered wireless smart sensor based on maglev porous nanogenerator for train monitoring system

Long Jin[a], Weili Deng[a], Yuchen Su[a], Zhong Xu[a], Huan Meng[a], Bin Wang[a], Hepeng Zhang[a], Binbin Zhang[a], Lei Zhang[a], Xinbiao Xiao[b], Minhao Zhu[a,b], Weiqing Yang[a,b,*]

[a] Key Laboratory of Advanced Technologies of Materials (Ministry of Education), School of Materials Science and Engineering, Southwest Jiaotong University, Chengdu 610031, PR China
[b] State Key Laboratory of Traction Power, Southwest Jiaotong University, Chengdu 610031, PR China

ARTICLE INFO

Keywords:
Triboelectric nanogenerator
Electromagnetic generator
Wireless sensor
Self-powered
Train monitoring

ABSTRACT

With the rapid development of high speed railway all around the world, the real-time monitoring is absolutely necessary for the safety running of high speed train. However, traditional monitoring method requires external power supply, and wired system makes the monitoring messy. Here, we reported a self-powered wireless smart sensor, powered by vibration energy of trains via a maglev porous nanogenerator (MPNG) when the train is running. Integrated MPNG including a triboelectric nanogenerator (TENG), which delivers a peak power density of 0.34 mW/g at 50 MΩ, and an electromagnetic generator (EMG), which delivers a peak power density of 0.12 mW/g at 700 Ω. Through a power management circuit (PMC), the MPNG is proved to power 400 commercial light-emitting diodes (LEDs). What's more, various supercapacitors and Li-ion battery can be charged by MPNG arrays, where the supercapacitor of 0.1 F can be charged from 0 V to 3 V in approximately 350 s. A wireless smart sensor can be sustainably powered by MPNG arrays, transmitting real-time data to a cellphone, demonstrating the capability for Internet of Things, especially in the train monitoring system.

1. Introduction

Train monitoring methods have been increasingly enriched along with the development of high speed railway system [1,2]. Combining Internet of Things with train monitoring becomes a tendency [3]. However, an external power source, such as a supercapacitor or Li-ion battery, is needed for sensors and other electronics for communications. As time goes by, this kind of traditional power supply mode becomes more and more unpractical and unfavorable, mainly for the limited battery lifetime, large scope, messy arrangement of wires and potential environmental hazards [4–6]. In this regard, an ideal solution is to use an energy harvester instead of battery, realizing a self-powered monitoring system.

Vibration, as one of the most attractive energy sources, is proved to be availably harvested [7–11]. What's more, the vibration induced by train is badly common while the train is running, resulting an enormous potential in energy harvesting. Generally, there are several methods for energy converting, including electromagnetic [12–14], piezoelectric [15–20], triboelectric [21–27], and electrostatic [28] effects. More recently, the triboelectric nanogenerator (TENG) [29–35] has been highlighted due to its simplicity, low cost, and light weight. In TENG, by utilizing the conjunction of contact electrification and electrostatic induction, a periodic contact and separation between two materials with different charge affinities drives induced electrons to move between two electrodes through an external resistance [36–42]. Compared to electromagnetic generator (EMG), TENG has a high voltage with a low current. In contrast, EMG has a low voltage with a high current. What's more, TENG has a high power density, but it is limited to power some larger devices sustainably. By integrating two energy convert units [43–45], a higher power density unit has been proved to power many devices sustainably.

In this work, we have developed a maglev porous nanogenerator (MPNG), integrating a TENG and an EMG, which is proved to harvest vibration energy from trains for wireless smart sensors. The device has a maglev structure, effectively combining TENG and EMG. The bottom magnet suspends the middle magnet due to the magnetic force, causing the space between two triboelectric materials for TENG working. Thus, TENG and EMG can work together. On the other hand, the well-designed structure makes the working frequency of MPNG match more closely with the frequency of the train when it is running. It is worth

* Corresponding author at: Key Laboratory of Advanced Technologies of Materials (Ministry of Education), School of Materials Science and Engineering, Southwest Jiaotong University, Chengdu 610031, PR China.
E-mail address: wqyang@swjtu.edu.cn (W. Yang).

http://dx.doi.org/10.1016/j.nanoen.2017.05.018
Received 31 March 2017; Received in revised form 8 May 2017; Accepted 8 May 2017
Available online 22 May 2017

mentioning that the Polytetrafluoroethylene (PTFE) of TENG is porous electret, enhancing the property of triboelectricity in some degree. Through a power management, MPNG can power about 400 commercial light-emitting diodes (LEDs) continuously. What's more, charging supercapacitors and Li-ion battery up to 3 V when connected to the wireless smart sensor has been proved. And the real-time data can be transmitted to cellphone. Individually, TENG delivers a power density of 0.34 mW/g, while EMG delivers a power density of 0.12 mW/g. In the long term, this work can push forward a revolutionary step toward train monitoring system without external power source or messy arrangement of wires.

2. Results and discussion

Fig. 1a illustrates the schematic diagram of developed smart sensor applied in the bogies by using the energy converted from the train vibration in train-running process. As a convenience, the signal submitted from the smart sensor can be receipted indoor, for example in the operation room. Bogies (shown in Fig. 1b) are the most important for safety monitoring of the train system. As demonstrated in Fig. 1c, energy is harvested from train vibration by MPNG arrays placed on the bogies for the wireless smart sensor (Fig. 1d) through a power management system (Fig. 1e). In the power management, the

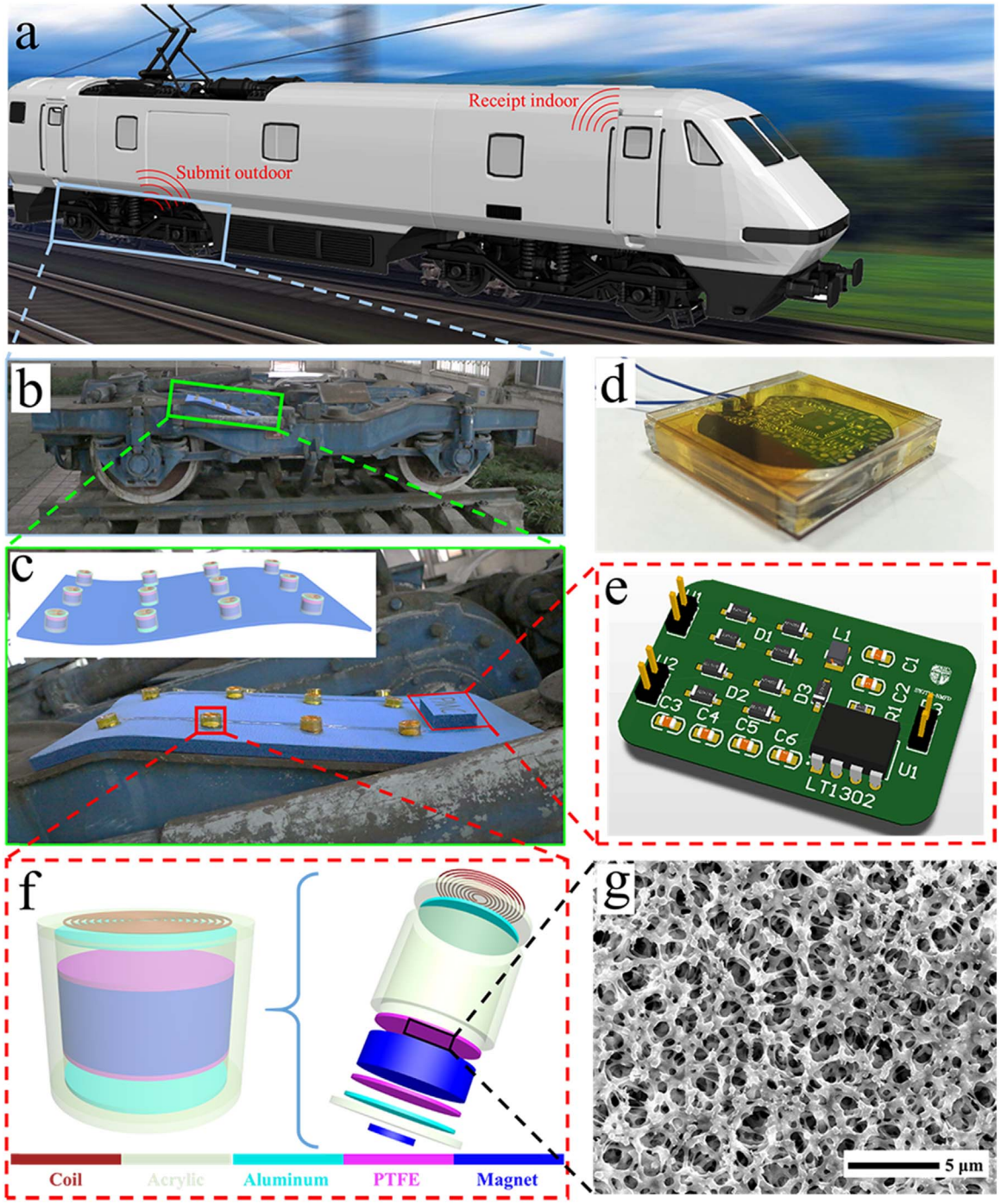

Fig. 1. Structural design of self-powered wireless smart sensor applied in train monitoring system. (a) Schematic illustration of the developed smart sensor applied in (b) the bogies by using the energy converted from the train vibration in train-running process. Energy harvested by (c) MPNG array, and then powers (d) the wireless smart sensor through (e) the power management circuit. (f) A general illustration and detailed structure of MPNG. (g) SEM image showing the polymer porous structure of the PTFE.

separated alternating current (AC) from TENGs and EMGs of MPNGs respectively can be transformed to direct current (DC), and then pre-stored together in supercapacitors. Finally, the smart sensor can be powered when connected to the power management circuit (PMC). The individual MPNG structure design is illustrated in Fig. 1f. Two aluminum foils on the substrates and two pieces of porous PTFE on both sides of the middle magnet constitute a typical TENG. In case of EMG, it consists of a bottom magnet, a middle magnet and a copper circuit on the upper substrate sequentially. A detailed schematic illustration of the fabrication diagram is presented in Fig. S1. To enhance the electrical performance of TENG, porous PTFE is applied as triboelectric material. A scanning electron microscopy (SEM) image of porous PTFE film is presented in Fig. 1f. The porous structure provides a rough surface, leading to a larger effective contact area when TENG is working. Thus, the output of electrical performance is improved. Furthermore, the inside micro hole of the porous PTFE improves the charge storage stability, signifying a long working lifetime and working stability [46–48].

Working principle can be described as movement of the middle magnet briefly, as shown in Fig. 2a. At first, the bottom PTFE on the middle magnet is connected fully with the bottom Al electrode, which results in no current in the coil or the peripheral circuit. When the middle magnet with PTFE moves up on account of the external vibration, the electrons can be injected from the upper Al electrode to the bottom electrode through the peripheral circuit due to the different triboelectric polarities. In this process, the magnetic flux of the coil varies because of the decreasing distance between the upper coil and the middle magnet, resulting in the current in the coil. Then, the magnet continues moving up, and there will be a full connect between the PTFE on the upper side of magnet and the upper aluminum electrode. When they connect fully, there is a balance on the electric potential between PTFE and the aluminum electrode. Hence, the electron will not move. And there is no change about the flux of the coil, resulting no current. In the following process, similar to the previous process, PTFE and Al electrode start to separate, leading to the imbalance on electric potential. The electron will be injected from the bottom electrode to the upper one. Meanwhile, according to Lenz's law, an opposite current in direction can be generated in the coil. Finally, the PTFE on the magnet has a full connect with the bottom Al electrode, the same as the initial state and completing a whole cycle of electricity generation. To accurately elucidate the working principle, COMSOL Multiphysics was employed to simulate the magnetic field and electrostatic field distributions of MPNG in Fig. 2b and c respectively. The magnetic poles of two magnets are set as Fig. S2. As a consequence, via delivering AC by TENG and EMG, the MPNG is capable to convert vibration energy to electricity. A dynamic principle can be seen in Movie 1.

Supplementary material related to this article can be found online at doi:10.1016/j.nanoen.2017.05.018.

To systematically investigate the output performance of the fabricated MPNG in harvesting vibration energy, a standard vibration shaker system has been employed as a shake source with available frequencies. As demonstrated in Fig. S3, TENG has a peak open-circuit voltage measured 43.8 V under 20 Hz with a peak short-circuit current of 1.39 μA. In addition, the half width of TENG is about 20 Hz, indicating a relatively wide frequency range to harvest energy. Under 20 Hz, Fig. S4a and b show open-circuit voltage and short-circuit current curves respectively. To obtain the optimum output power, the output voltage and current are measured under various external load resistances. As depicted in Fig. 3a, the output current reduces, while the output voltage increases with the gradually increased resistances. Especially ranging from 1 MΩ to 1 GΩ, the change is sharp. Similar to TENG, EMG shows a half width of 19 Hz both in voltage and current, as demonstrated in Fig. S5. EMG can deliver a peak voltage of 7.7 V (Fig. S6a) and a peak current of 4.1 mA (Fig. S6b). Compared with TENG, the matched resistance of EMG is lower. Fig. 3b shows that the voltage and current change sharp between 100 Ω and 100 kΩ. Instantaneous peak power density (calculated by $P_d = I^2R/M$, as shown in Supporting Information) is plotted in Fig. 3c (TENG) and Fig. 3d (EMG). At a resistance of 50 MΩ, TENG has a peak power density of 0.34 mW/g, while EMG delivers a peak power density of 0.12 mW/g at 700 Ω.

To explore the adaptive capacity to environment further, MPNG has been rinsed by water. As demonstrated in Fig. 3e, water has hardly influenced the output of TENG. The same as TENG, the performance of EMG reduces barely, as presented in Fig. 3f. For a visual demonstra-

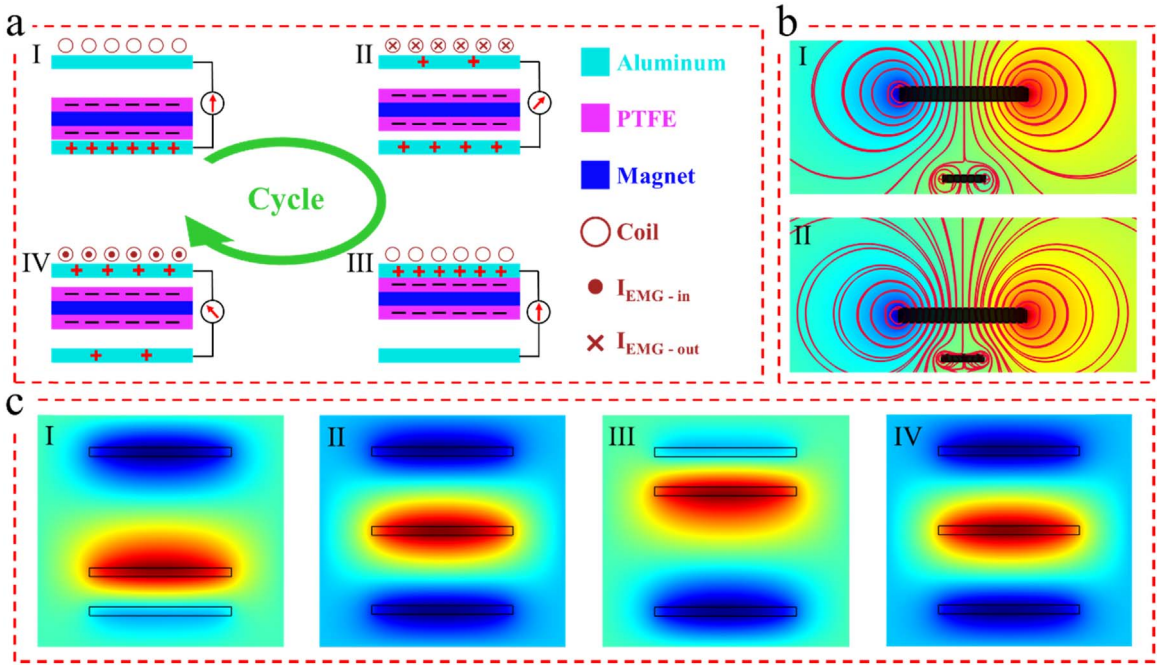

Fig. 2. Electricity generation process of the MPNG. (a) Schematic diagram of MPNG including TENG and EMG. Simulation of (b) magnetic field and (c) electrostatic field employed by COMSOL Multiphysics for elucidation.

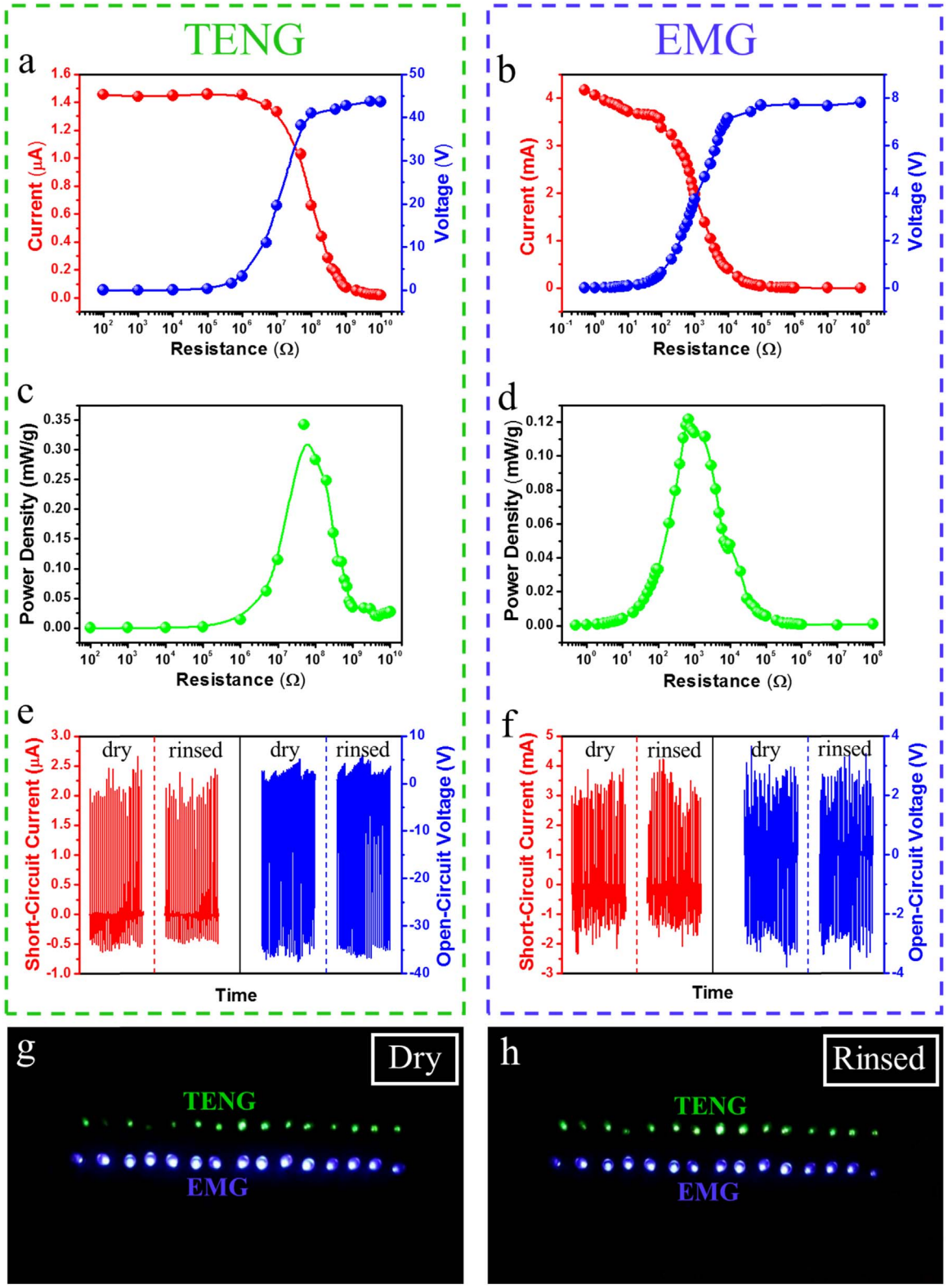

Fig. 3. Output performance of the fabricated MPNG. Measured output voltage and current signal of the (a) TENG and (b) EMG on the different external loading resistances. Calculated power density of the (c) TENG and (d) EMG on the different external loading resistances. Comparison of short-circuit current and open-circuit voltage between (e) dry MPNG and (f) the one after rinsing by water. The LEDs lighted by (g) dry MPNG and the one after rinsing by water.

tion, LEDs lighted by MPNG are applied. The green LEDs are lighted by TENG, while the blue LEDs are lighted by EMG, as shown in Fig. 3g, h and Movie 2. There are few differences between brightness of LEDs lighted by dry MPNG and the one after rinsing, clearly presenting the excellent environmental stability of MPNG.

Supplementary material related to this article can be found online at doi:10.1016/j.nanoen.2017.05.018.

Electrical energy is often stored in energy storage devices, so an exploration about charging capability of MPNG is applied. Fig. 4a presents a circuit diagram of the PMC. If the charging energy storage is

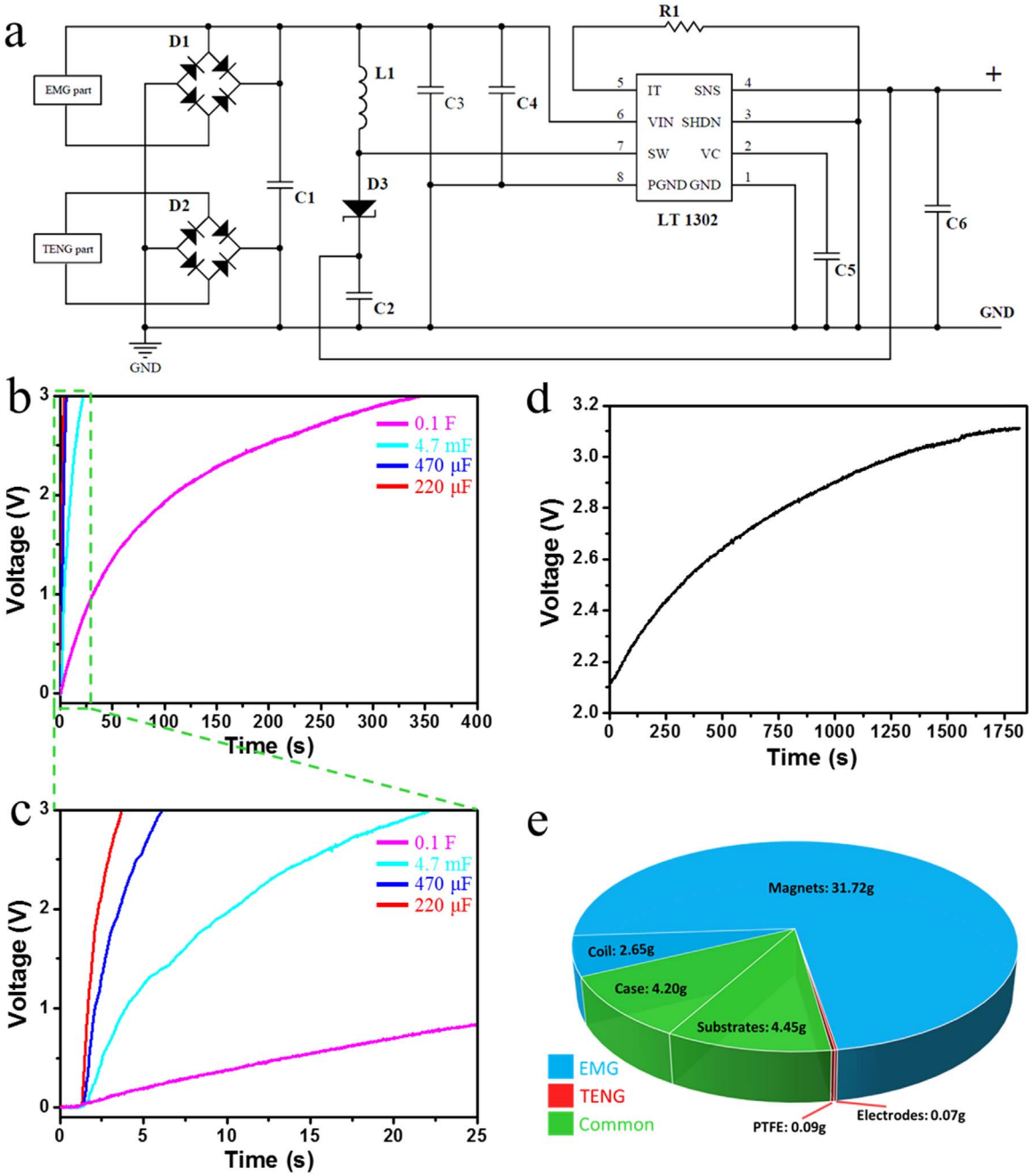

Fig. 4. Charging characteristics of the MPNG. (a) Circuit diagram of the power management system. (b) Voltage curves of charging different supercapacitors and (c) enlarged view showing different charging rate on different supercapacitor. (d) Voltage curve showing the cycle of a Li-ion battery. (e) Individual mass fractions of the MPNG.

directly connected to electronics through rectifiers, the supplied power gradually decreases as the discharging processes. Therefore, a power management system is necessary. Fig. 4a presents the PMC, including a pre-store device, DC-DC converter, and a capacitor for stable output. Usually, supercapacitor is a good choice for its rapid charge and discharge [49–51]. Voltage curves of charging different supercapacitors are presented in Fig. 4b, c by MPNG arrays through PMC, where the supercapacitor of 0.1 F can be charged from 0 V to 3 V in approximately 350 s. What's more, the charge curves of different supercapacitors vary, as presented detailedly in Fig. 4c. On the other hand, Li-ion battery [52], as the most commonly used energy storage device, can be charged effectively by MPNG via PMC, shown in Fig. 4d. From 2.1 V, below the safety voltage, Li-ion battery can be charged to about 3.1 V in about 1800 s, where most electronics can work well. As an addition, MPNG has a light weight of 43.18 g, where individual mass fractions of MPNG are displayed in Fig. 4e. Magnets of 31.72 g and the coil of 2.65 g are only used by EMG, PTFE of 0.09 g and electrodes of 0.07 g are only used by TENG, and the common part including case of 4.20 g and substrates of 4.45 g, where can be seen that TENG is much lighter than EMG. In response to this, the power density of TENG (Fig. 3c) is higher than EMG (Fig. 3d).

For application in bogies of train, MPNG arrays were fabricated and the corresponding self-powdered wireless smart sensor were demonstrated in Fig. 5a. Fig. 5b shows the desirable bendability MPNG arrays, illustrating some degree of bendability, which is more adaptive in shapes. Furthermore, it is more convenient to be carried. As a consequence, the wireless smart sensor (Fig. 5c) can be powered sustainably. In detail, Fig. 5d shows a typical charge curve at first, where the supercapacitor of 4.7 mF can be charged from 0 V to 3.3 V in about 29 s. When the wireless smart sensor is turned on, the curve of

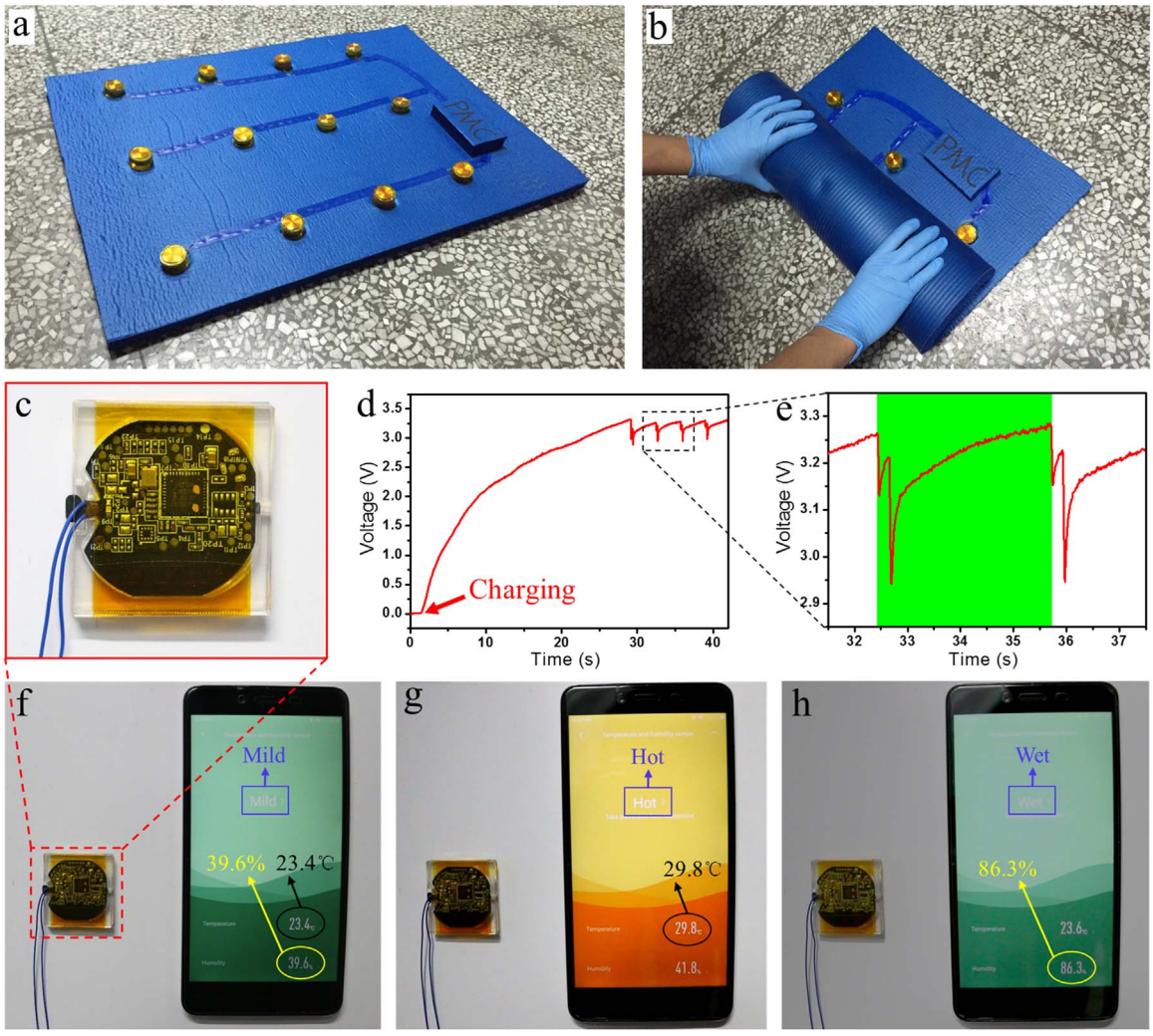

Fig. 5. Demonstrate of wireless smart sensor powered by MPNGs. Photographs of (a) the array of MPNG and (b) the bended one. (c) Photograph of wireless smart sensor. (d) Charging curve and (e) the enlarged one of a 4.7 mF supercapacitor connected to sensor. Photographs (f) when the sensor is working, (g) after heated, and (h) after humidified powered.

voltage starts to drop and then rises again. The green part in Fig. 5e, an enlarged view, presents a whole cycle. The decreasing curve indicates that data is transmitted, and the consumption is larger than the produced electricity energy by MPNG arrays. After transmitting, the curve turns back to 3.3 V, owing to the lower power consumption. As shown in Fig. 5f, the cellphone displays the indoor environment parameters with a temperature of 23.4 °C and humidity of 39.6%, and the environment is wild. After heated by hot-wind blower, the temperature turns to 29.8 °C, with the degree of comfort becomes hot, as displayed in Fig. 5g and Movie 3. Finally, after breathing to it by human, the humidity increases sharply, and the cellphone exhibits the word of wet and 86.3% (shown in Fig. 5h and Movie 4). What's more, MPNG arrays can also power LEDs as a power supply (shown in Fig. S7 and Movie 5).

Supplementary material related to this article can be found online at doi:10.1016/j.nanoen.2017.05.018.

3. Conclusion

In summary, we have demonstrated a MPNG including a TENG and an EMG to harvest vibration energy of trains for sustainably powering a wireless smart sensor. Under a frequency of 20 Hz, TENG has a peak open-circuit voltage of 43.8 V and short-circuit current of 1.39 μA, as well as EMG's maximal open-circuit voltage of 7.7 V and short-circuit current of 4.1 mA. Connected to external resistance, TENG can deliver a peak power density of 0.34 mW/g at 50 MΩ, while EMG has a maximal power density of 0.12 mW/g at 700 Ω. After integrated, MPNG can charge various supercapacitors and Li-ion battery through PMC. When connected to the PMC with MPNG arrays, wireless smart sensor can transmit data to cellphone, showing temperature and humidity. What's more, MPNG can also power LEDs for illumination as an emergency power supply. This designed MPNG has a potential for wireless monitoring without external power supply, especially in the train monitoring system.

4. Experimental section

4.1. Fabrication of the device

The frame work of this device was structured by two acrylic substrates and an acrylic tube. First, two acrylic sheets were fabricated by using a laser cutter as substrates. Secondly, a small magnet was placed in the bottom substrate, and a piece of aluminum foil was fixed on the top side of the bottom substrate. Then, a cylinder magnet above

the bottom substrate was fixed with porous Polytetrafluoroethylene (PTFE) on the two sides. Next, the acrylic tube was placed, coving the magnet. Finally, another aluminum foil and a copper coil was fixed on the two sides of the other acrylic substrate. As a result, the device is composed of a triboelectric nanogenerator (TENG) and an electromagnet generator (EMG) within a one-body package.

4.2. Measurement of the device

The output voltage signals were measured by a low-noise voltage preamplifier (Keithley 6514 system electrometer). The output current voltage signals were measured by a low-noise current preamplifier (Stanford Research SR570). The vibration source was generated by a vibration shaker (DONGLING TECH ESS-025). The microstructure of surface was observed by SEM (JEOL JSM-7001F).

Acknowledgments

This work was supported by the National Natural Science Foundation of China (No. 51602265), the Scientific and Technological Projects for Distinguished Young Scholars of Sichuan Province (No. 2015JQ0013), China Postdoctoral Science Foundation (No. 2016M592692), the Fundamental Research Funds for the Central Universities of China (No. A0920502051619-72) and the Independent Research Project of State Key Laboratory of Traction Power (Nos. 2017TPL_Z04 and 2016TPL_Z03).

Appendix A. Supporting information

Supplementary data associated with this article can be found in the online version at doi:10.1016/j.nanoen.2017.05.018.

References

[1] G. Lederman, S.H. Chen, J.H. Garrett, J. Kovacevic, H.Y. Noh, J. Bielak, Mech. Syst. Signal Process. 90 (2017) 141–153.
[2] L.Q. Wang, Y. Zhang, S.T. Lie, J. Sound Vib. 392 (2017) 142–153.
[3] C. Ling, R.P.B.J. Dollevoet, R.F. Hanssen, IEEE J. Sel. Top. Appl. Earth Obs. Remote Sens. 10 (2017) 596–604.
[4] M.-L. Seol, J.-W. Han, S.-J. Park, S.-B. Jeon, Y.-K. Choi, Nano Energy 23 (2016) 50–59.
[5] G. Zhu, W.Q. Yang, T. Zhang, Q. Jing, J. Chen, Y.S. Zhou, P. Bai, Z.L. Wang, Nano Lett. 14 (2014) 3208–3213.
[6] G. Zhu, Y. Su, P. Bai, J. Chen, Q. Jing, W. Yang, Z.L. Wang, ACS Nano 8 (2014) 6031–6037.
[7] C. Wu, R. Liu, J. Wang, Y. Zi, L. Lin, Z.L. Wang, Nano Energy 32 (2017) 287–293.
[8] X. Xia, G. Liu, H. Guo, Q. Leng, C. Hu, Y. Xi, Nano Energy 15 (2015) 766–775.
[9] Q. Liang, Z. Zhanga, X. Yan, Y. Gu, Y. Zhao, G. Zhang, S. Lu, Q. Liao, Y. Zhang, Nano Energy 14 (2015) 209–216.
[10] J. Chen, Y. Huang, N. Zhang, H. Zou, R. Liu, C. Tao, X. Fan, Z.L. Wang, Nat. Energy 1 (2016) 16138.
[11] J. Chen, G. Zhu, W. Yang, Q. Jing, P. Bai, Y. Yang, T.C. Hou, Z.L. Wang, Adv. Mater. 25 (2013) 6094–6099.
[12] X. Bai, Y. Wen, J. Yang, P. Li, J. Qiu, Y. Zhu, J. Appl. Phys. 111 (2012) 07A938.
[13] I. Sari, T. Balkan, H. Kulah, Sens. Actuators A: Phys. 145–146 (2008) 405–413.
[14] S.P. Beeby, R.N. Torah, M.J. Tudor, P. Glynne-Jones, T.O. Donnell, C.R. Saha, S. Roy, J. Micromech. Microeng. 17 (2007) 1257.
[15] R. Yu, C. Pan, J. Chen, G. Zhu, Z.L. Wang, Adv. Funct. Mater. 23 (2013) 5868–5874.
[16] Y. Hu, Z.L. Wang, Nano Energy 14 (2015) 3–14.
[17] T. Huang, C. Wang, H. Yu, H. Wang, Q. Zhang, M. Zhu, Nano Energy 14 (2015) 226–235.
[18] N. Soin, P. Zhao, K. Prashanthi, J. Chen, P. Ding, E. Zhou, T. Shah, S.C. Ray, C. Tsonos, T. Thundat, Nano Energy 30 (2016) 470–480.
[19] C. Xu, L. Zhang, Y. Xu, Z. Yin, Q. Chen, S. Ma, H. Zhang, R. Huang, C. Zhang, L. Jin, W. Yang, J. Lu, J. Mater. Chem. A 5 (2017) 189–200.
[20] Z.L. Wang, J.H. Song, Science 312 (2006) 242–246.
[21] L. Zhang, B. Zhang, J. Chen, L. Jin, W. Deng, J. Tang, H. Zhang, H. Pan, M. Zhu, W. Yang, Z.L. Wang, Adv. Mater. 28 (2015) 1650–1656.
[22] L. Zhang, L. Jin, B. Zhang, W. Deng, H. Pan, J. Tang, M. Zhu, W. Yang, Nano Energy 16 (2015) 516–523.
[23] H. Zhang, S. Zhang, G. Yao, Z. Huang, Y. Xie, Y. Su, W. Yang, C. Zheng, Y. Lin, ACS Appl. Mater. Interfaces 7 (2015) 28142–28147.
[24] J. Chen, G. Zhu, J. Yang, Q. Jing, P. Bai, W. Yang, X. Qi, Y. Su, Z.L. Wang, ACS Nano 9 (2015) 105–116.
[25] W.Q. Yang, J. Chen, G. Zhu, J. Yang, P. Bai, Y.J. Su, Q.S. Jing, X. Cao, Z.L. Wang, ACS Nano 7 (2013) 11317–11324.
[26] W. Yang, J. Chen, G. Zhu, X. Wen, P. Bai, Y. Su, Y. Lin, Z. Wang, Nano Res. 6 (2013) 880–886.
[27] J. Chen, J. Yang, Z. Li, X. Fan, Y. Zi, Q. Jing, H. Guo, Z. Wen, K.C. Pradel, S. Niu, Z.L. Wang, ACS Nano 9 (2015) 3324–3331.
[28] P.D. Mitcheson, P. Miao, B.H. Stark, E.M. Yeatman, A.S. Holmes, T.C. Green, Sens. Actuators A: Phys. 115 (2004) 523–529.
[29] Y. Su, G. Zhu, W. Yang, J. Yang, J. Chen, Q. Jing, Z. Wu, Y. Jiang, Z.L. Wang, ACS Nano 8 (2014) 3843–3850.
[30] X. Wen, W. Yang, Q. Jing, Z.L. Wang, ACS Nano 8 (2014) 7405–7412.
[31] W. Yang, J. Chen, Q. Jing, J. Yang, X. Wen, Y. Su, G. Zhu, P. Bai, Z.L. Wang, Adv. Funct. Mater. 24 (2014) 4090–4096.
[32] Z.L. Wang, ACS Nano 7 (2013) 9533–9557.
[33] J. Chen, J. Yang, H. Guo, Z. Li, L. Zheng, Y. Su, Z. Wen, X. Fan, Z.L. Wang, ACS Nano 9 (2015) 12334–12343.
[34] G. Zhu, J. Chen, T. Zhang, Q. Jing, Z.L. Wang, Nat. Commun. 5 (2014) 3426.
[35] W. Yang, J. Chen, X. Wen, Q. Jing, J. Yang, Y. Su, G. Zhu, W. Wu, Z.L. Wang, ACS Appl. Mater. Interfaces 6 (2014) 7479–7484.
[36] S. Niu, Z.L. Wang, Nano Energy 14 (2015) 161–192.
[37] X.-S. Zhang, M.-D. Han, R.-X. Wang, B. Meng, F.-Y. Zhu, X.-M. Sun, W. Hu, W. Wang, Z.-H. Li, H.-X. Zhang, Nano Energy 4 (2014) 123–131.
[38] L. Xu, Y. Pang, C. Zhang, T. Jiang, X. Chen, J. Luo, W. Tang, X. Cao, Z.L. Wang, Nano Energy 31 (2017) 351–358.
[39] L. Su, H.Y. Li, Y. Wang, S.Y. Kuang, Z.L. Wang, G. Zhu, Nano Energy 31 (2017) 264–269.
[40] Y.H. Kwon, S.-H. Shin, Y.-H. Kim, J.-Y. Jung, M.H. Lee, J. Nah, Nano Energy 25 (2016) 225–231.
[41] W. Deng, L. Jin, B. Zhang, Y. Chen, L. Mao, H. Zhang, W. Yang, Nanoscale 8 (2016) 16302–16306.
[42] W. Deng, B. Zhang, L. Jin, Y. Chen, W. Chu, H. Zhang, M. Zhu, W. Yang, Nanotechnology 28 (2017) 135401.
[43] L. Jin, J. Chen, B. Zhang, W. Deng, L. Zhang, H. Zhang, X. Huang, M. Zhu, W. Yang, Z.L. Wang, ACS Nano 10 (2016) 7874–7881.
[44] B. Zhang, J. Chen, L. Jin, W. Deng, L. Zhang, H. Zhang, M. Zhu, W. Yang, Z.L. Wang, ACS Nano 10 (2016) 6241–6247.
[45] H. Zhang, J. Wang, Y. Xie, G. Yao, Z. Yan, L. Huang, S. Chen, T. Pan, L. Wang, Y. Su, W. Yang, Y. Lin, ACS Appl. Mater. Interfaces 8 (2016) 32649–32654.
[46] X. Zhang, G.M. Sessler, Y. Xue, X. Ma, J. Phys. D Appl. Phys. 49 (2016) 205502.
[47] Z. Xia, A. Wedel, R. Danz, IEEE Trans. Dielectr. Electr. Insul. 10 (2003) 102–108.
[48] Z. Xia, A. Buechtemann, Z. An, J. Jiang, R. Danz, A. Wedel, J. Electrost. 63 (2005) 387–398.
[49] H. Zhang, H. Su, L. Zhang, B. Zhang, F. Chun, X. Chu, W. He, W. Yang, J. Power Sources 331 (2016) 332–339.
[50] H. Zhang, L. Zhang, J. Chen, H. Su, F. Liu, W. Yang, J. Power Sources 315 (2016) 120–126.
[51] L. Zhang, H. Zhang, L. Jin, B. Zhang, F. Liu, H. Su, F. Chun, Q. Li, J. Peng, W. Yang, RSC Adv. 6 (2016) 50209–50216.
[52] H. Zhang, X. Sun, X. Zhang, H. Lin, K. Wang, Y. Ma, J. Alloy. Compd. 622 (2015) 783–788.

Long Jin received his B.E. from Southwest Jiaotong University in 2015. He is currently pursuing Ph.D. degree in materials science and engineering at Southwest Jiaotong University.

Weili Deng received his B.S. degree in electronic science and technology from Chongqing University in 2006, and then earns his master degree in 2009. Now he is a doctor in materials science and engineering at Southwest Jiaotong University.

Yuchen Su is a junior student in University of Materials Science and Engineering of China. She majors in Polymer Materials. Her recent research interest is nanogenerator and related applications.

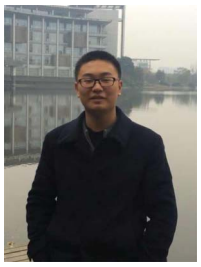

Zhong Xu is a junior student in Southwest Jiaotong University of China. He mayors in Materials Science and Engineering. His recent research focus on nanogenerators and flexible supercapacitors.

Huan Meng is a junior student in Southwest Jiaotong University. He majors in Rail traffic signal and control. He is dedicated to Freescale cup national college students intelligent car race.

Bin Wang is a junior student in Southwest Jiaotong University. He majors in Polymer Materials. His recent research interest is nano energy materials and devices.

Hepeng Zhang is a graduate student in University of Southwest Jiaotong University of China. He majors in Materials Science and Engineering. His recent research interest is nanogenerator and related applications.

Binbin Zhang received his B.E. from Southwest Jiaotong University in 2015. He is currently pursuing a Ph.D. degree in materials science and engineering at Southwest Jiaotong University under the guidance of Professor Weiqing Yang.

Lei Zhang received her B.E. degree in polymer material engineering from Chongqing University of Arts and Science in 2014. He is a graduate student in materials science and engineering at Southwest Jiaotong University under the guidance of Professor Weiqing Yang. His research focuses on the triboelectric nanogenerator and supercapacitor.

Xinbiao Xiao received his B.E. in engineering mechanics in 2002, M.S. in 2005, and Ph.D. in 2013 from Southwest Jiaotong University. Now he is the associate research fellow of Southwest Jiaotong University. His current research focuses on vibration and noise of rail transportation.

Minhao Zhu received his B.E. in metal materials science and engineering in 1990, M.S. in 1993, and Ph.D. in 2001 from Southwest Jiaotong University. Now he is the professor of Southwest Jiaotong University, Yangtze River Scholar Distinguished Professor of China and National Outstanding Youth Fund Gainer. His current research focuses on Materials Science and Engineering, Mechanical Design and Theory.

Weiqing Yang received his M.S. in Physics in 2007, and Ph.D. in Materials Science and Engineering from Sichuan University in 2011. He was a post-doctorate research fellow at University of Electronic Science and Technology of China from 2011 to 2013. Subsequently, he was a post-doctorate research fellow at Georgia Institute of Technology from 2013 to 2014, under the supervision of Prof. Zhong Lin Wang. Now he is a professor at South Jiaotong University and his research focuses on nano energy materials and micro/nano devices.